Zhuyun Xu
Postdoctorate
e-mail: zxu@blwtl.uwo.ca

Horia Hangan
Associate Professor
Associate Research Director
e-mail: hmh@blwtl.uwo.ca

The Boundary Layer Wind Tunnel Laboratory,
University of Western Ontario,
Ontario N6A 5B9, Canada

Pei Yu
Professor
Department of Applied Mathematics,
University of Western Ontario,
Ontario N6A 5B7 Canada
e-mail: pyu@uwo.ca

Analytical Solutions for a Family of Gaussian Impinging Jets

Various types of impinging jet flows are analytically modeled using inviscid free Gaussian jet solutions superimposed with experimentally fitted boundary layer models. Improved (more robust) and simplified solutions to existing models are defined. Velocity profiles, surface pressure distributions, and streamline plots are calculated for circular, plane, and annular impinging jets. The models show excellent agreement with existing experimental results in both laminar and turbulent conditions and for different Reynolds numbers.
[DOI: 10.1115/1.2775502]

Keywords: impinging jets, analytical models

1 Introduction

Impinging jets have extensive practical applications ranging from industrial processing, such as mixing, heating/cooling, or drying, to environmental flows related to ventilation or the simulation of downburst winds. The mathematical modeling of the flow field has therefore both fundamental and practical importance.

A three region modeling method for round impinging jets was put forward and the flow field of the wall jet region was broadly investigated [1–3]. The normalized radial velocity profile derived by Glauert [1] and verified by Bakke [2] is often cited in many references. However, it cannot be used to predict the flow field in the impinging jet region.

Yih [4] obtained a solution of steady rotational flow equations of an inviscid fluid describing rapidly varying flows such as flows from a two-dimensional channel or a circular tube toward a sink. A similar solution for an impinging jet was found by Phares et al. [5]. They derived a double layer summarized infinite series solution that includes surface integrals to be computed numerically. The solution can be considered as an analytical-numerical mixed solution.

In 1998, Lee et al. [6] derived a pure analytical solution for a simple Gaussian impinging jet and applied the solution to the flow field research for helicopter vanes.

Herein, we improve the analytical model of Lee et al. and extend it to the general case of a family of Gaussian impinging jets. The extended solution is more adequate for modeling an extended set of engineering problems involving round impinging jets [7]. A direct solution for the steady rotational flow equations subject to the inhomogeneous boundary conditions is obtained. An approximate method for computing the oscillatory series of the solution is proposed and proved suitable for general oscillatory series. Based on this, a complete flow field of the Gaussian impinging jets can be readily computed. The approximate solution for the oscillatory series accelerates convergence and adds robustness to the model when compared to previous ones.

Contributed by the Applied Mechanics Division of ASME for publication in the JOURNAL OF APPLIED MECHANICS. Manuscript received February 19, 2007; final manuscript received July 19, 2007; published online February 27, 2008. Review conducted by Nesreen Ghaddar.

2 Formulation

2.1 Governing Equations and Boundary Conditions. In accordance with the formulation of Lee et al. [6], all lengths are nondimensionalized with jet radius R^* (or half-width of the slot B_0^* for the plane jet) and all velocities are nondimensionalized with the maximum influx velocity w_m. Flow field pressures are nondimensionalized by the maximum dynamic pressure at the jet centerline. To simplify notations, the dimensional variables are marked with $*$. The dimensionless variables are given as

$$r = \frac{r^*}{R^*} \quad z = \frac{z^*}{R^*} \quad \text{for round jets and}$$
$$x = \frac{x^*}{B_0^*} \quad z = \frac{z^*}{B_0^*} \quad \text{for plane jets} \tag{1}$$

$$u = \frac{u^*}{w_m} \quad w = \frac{w^*}{w_m} \quad p = \frac{2p^*}{\rho w_m^2} \tag{2}$$

The governing equations written in stream function and vorticity form are

$$\frac{\partial^2 \psi}{\partial z^2} + \frac{\partial^2 \psi}{\partial r^2} - \frac{1}{r}\frac{\partial \psi}{\partial r} = -r^2 \Omega(r,z) \tag{3}$$

$$\frac{\partial \psi}{\partial r} = rw \quad \frac{\partial \psi}{\partial z} = -ru \tag{4}$$

$$\Omega = \frac{1}{r}\left(\frac{\partial u}{\partial z} - \frac{\partial w}{\partial r}\right) \tag{5}$$

in cylindrical-polar coordinates for the round jet case and

$$\frac{\partial^2 \psi}{\partial z^2} + \frac{\partial^2 \psi}{\partial x^2} = -\Omega(x,z) \tag{6}$$

$$\frac{\partial \psi}{\partial x} = w \quad \frac{\partial \psi}{\partial z} = -u \tag{7}$$

$$\Omega = \left(\frac{\partial u}{\partial z} - \frac{\partial w}{\partial x}\right) \tag{8}$$

in Cartesian coordinates for the plane jet case.

The boundary conditions can be approximately expressed according to a finite domain [5,6], but here, precise expressions can be used for an infinite domain:

$$\psi = \int_o^r r w_\infty dr \quad \text{at } z = \infty \tag{9}$$

$$\psi = 0 \quad \text{at } z = 0 \tag{10}$$

$$\psi = 0 \quad \text{at } r = 0 \tag{11}$$

$$\frac{\partial \psi}{\partial r} = 0 \quad \text{at } r = \infty \tag{12}$$

for the round jet case and

$$\psi = \int_o^x w_\infty dx \quad \text{at } z = \infty \tag{13}$$

$$\psi = 0 \quad \text{at } z = 0 \quad \text{and at } x = 0 \tag{14}$$

$$\frac{\partial \psi}{\partial x} = 0 \quad \text{or } \psi = \int_o^z - u_\infty dz \quad \text{at } x = \infty \tag{15}$$

for the plane jet case.

2.2 Influx Velocity Profiles. Several empirical expressions are available to describe the jet influx velocity profile as a function of the nozzle shape, the spacing between the jet outlet and the impinging surface, and the flow state. The following Gaussian jet profile:

$$- w_\infty = e^{-r^2/k} \tag{16}$$

is chosen because Eq. (9) has an exact solution with this influx velocity profile and the spacing distance (H^*) can be related to the final solution as well.

Firstly, in order to find a relation between Gaussian jets and a jet from a round pipe, their flow rates can be compared as follows.

Considering an influx flowing out from a pipe with $r=1$ and the uniform velocity distribution (step profile, $w_\infty=-1$ for $r \leqslant 1$, $w_\infty=0$ elsewhere):

$$Q_0 = \int_0^1 - 2\pi r dr = - \pi \tag{17}$$

Using the influx profile of Eq. (16) and integrating from $r=0$ to ∞, the flow rate corresponding to the Gaussian jet is obtained:

$$Q = \int_0^\infty w_\infty 2\pi r dr = \int_0^\infty - e^{-r^2/k} 2\pi r dr = - k\pi \tag{18}$$

Obviously, the Gaussian influx velocity profile (16) provides k times the unit flow rate (kQ_0).

Secondly, a turbulent jet produces flow entrainment into the shear layer, hence increasing its flow rate as it moves downward. In order to take into account the entrainment effects into the inviscid model, the relation between the flow rate multiplier (k) and the distance from the jet to the impinging plate (H^*) should be specified.

According to Abramovich's experiments for a free round turbulent jet (Ref. [8], pp. 20–26) the parameter k and the distance from the jet outlet to a downstream flow station (H^*) can be related by

$$k = \frac{Q}{Q_0} = 2.2\left(a_1 \frac{H^*}{R^*} + b_1\right) \tag{19}$$

where a_1 is a jet shape coefficient, typically taking $a_1=0.06-0.08$; b_1 is an empirical constant chosen as $b_1=0.294$; H^* is the axial distance from the jet exit.

Hence, in order to include the entrainment effects, a flow rate Q ($=kQ_0$) can be used as the influx. The parameter k can be regarded as a linkage between the infinite and finite domains and introduced into the model.

For the same reason, the following influx profile is chosen for the plane jet case:

$$- w_\infty = (1 + 2x/k)e^{-2x/k} \tag{20}$$

and an empirical expression for k is given by (Ref. [8], pp. 27–28)

$$k = \frac{Q}{Q_0} = 1.2\sqrt{\frac{a_2 H^*}{B_0^*} + b_2} \tag{21}$$

where a_2 is the jet shape coefficient, $a_2=0.10-0.11$; b_2 is an empirical constant, $b_2=0.41$.

2.3 Analytical Solutions for a Family of Gaussian Impinging Jets. An infinite series solution is obtained for the steady axial-symmetric flow (Eq. (3)) given the inhomogeneous mixed boundary conditions (Eqs. (9)–(12)) with the influx velocity profile (Eq. (16)).

(a) The stream function is

$$\psi = -\frac{k}{2}(1 - e^{-r^2/k}) + r^2 e^{-r^2/k} \sum_{n=1}^{\infty} c_n L_n^1\left(\frac{2r^2}{k}\right) e^{-\sqrt{8n/k}z} \tag{22}$$

with

$$c_n = \frac{\int_0^\infty (k/2)(1 - e^{-r^2/k}) L_n^1(2r^2/k) e^{-r^2/k} r dr}{\int_0^\infty r^2 e^{-2r^2/k} [L_n^1(2r^2/k)]^2 r dr} = \frac{(-1)^n}{n \times n!} \tag{23}$$

where $L_n^1(x)$ are associated Laguerre polynomials.

As r and z are small, the solution shows that $\psi \sim z r^2$.

The velocity solutions are as follows:

(b) The radial velocity is

$$u(r,z) = r e^{-r^2/k} \sum_{n=1}^{\infty} c_n L_n^1\left(\frac{2r^2}{k}\right) \sqrt{8n/k} e^{-\sqrt{8n/k}z} \tag{24}$$

(c) The axial velocity is

$$w(r,z) = - e^{-r^2/k} + 2\left(1 - \frac{r^2}{k}\right) e^{-r^2/k} \sum_{n=1}^{\infty} c_n L_n^1\left(\frac{2r^2}{k}\right) e^{-\sqrt{8n/k}z} + r e^{-r^2/k} \sum_{n=2}^{\infty} c_n e^{-\sqrt{8n/k}z} \frac{\partial L_n^1(2r^2/k)}{\partial r} \tag{25}$$

For the particular cases of the plate surface ($z=0$) and the jet centerline ($r=0$), the associated velocities are obtained as

$$u(r,0) = r e^{-r^2/k} \sum_{n=1}^{\infty} c_n L_n^1\left(\frac{2r^2}{k}\right) \sqrt{\frac{8n}{k}} \tag{26}$$

$$w(0,z) = - 1 + 2\sum_{n=1}^{\infty} (-1)^{n-1} e^{-\sqrt{8n/k}z} \tag{27}$$

Lee et al. [6] provided a derivation for their solution of a simple Gaussian jet ($k=1$ in Eq. (16)) impinging onto a plate. In the following, we extend the result to the general case (k chosen arbitrarily).

Derivation. First, using Eq. (16) as the influx condition at $z=\infty$, the influx stream function can be expressed by

$$\psi_\infty = \int_0^r r(-e^{-r^2/k})dr = -\frac{k}{2}(1-e^{-r^2/k}) \tag{28}$$

The initial azimuthal vorticity distribution is defined by Eq. (5) as

$$\Omega = \Omega_\infty = -\frac{1}{r}\frac{\partial w_\infty}{\partial r} = -\frac{2}{k}e^{-r^2/k} \tag{29}$$

The conservation laws for axial-symmetric flow require Ω to be constant on streamlines [6], so that

$$\Omega = H(\psi) \tag{30}$$

The stream function ψ still satisfies Eq. (3) but now takes the special form

$$\frac{\partial^2\psi}{\partial z^2} + \frac{\partial^2\psi}{\partial r^2} - \frac{1}{r}\frac{\partial\psi}{\partial r} = -r^2H(\psi) \tag{31}$$

The azimuthal vorticity in the undisturbed jet at upstream infinity is given by Eq. (29). Making use of Eqs. (28) and (30), we have

$$H(\psi_\infty) = -\frac{4}{k^2}\left(\psi_\infty + \frac{k}{2}\right) \tag{32}$$

$H(\psi_\infty)$ is invariant throughout the flow field. Hence, Eq. (31) simplifies to a linear partial differential equation:

$$\frac{\partial^2\psi}{\partial z^2} + \frac{\partial^2\psi}{\partial r^2} - \frac{1}{r}\frac{\partial\psi}{\partial r} = \frac{4r^2}{k^2}\left(\psi + \frac{k}{2}\right) \tag{33}$$

Letting $\Psi = \psi + k/2$, Eq. (33) yields

$$\frac{\partial^2\Psi}{\partial z^2} + \frac{\partial^2\Psi}{\partial r^2} - \frac{1}{r}\frac{\partial\Psi}{\partial r} = \frac{4r^2}{k^2}\Psi \tag{34}$$

A particular solution of this equation for ψ is given by Eq. (28). The homogeneous equation can be solved by the method of separation of variables.

Letting $\Psi = F(r)\cdot G(z)$, then

$$F\frac{\partial^2 G}{\partial z^2} + G\frac{\partial^2 F}{\partial r^2} - \frac{G}{r}\frac{\partial F}{\partial r} - \frac{4r^2}{k^2}FG = 0 \tag{35}$$

The above equation can be rewritten into

$$\frac{1}{F}\frac{\partial^2 F}{\partial r^2} - \frac{1}{rF}\frac{\partial F}{\partial r} - \frac{4r^2}{k^2} = -\frac{1}{G}\frac{\partial^2 G}{\partial z^2} = \alpha \tag{36}$$

This leads to the following group equations:

$$G'' + \alpha G = 0 \tag{37}$$

$$F'' - \frac{1}{r}F' - \left(\frac{4r^2}{k^2} + \alpha\right)F = 0 \tag{38}$$

Letting $t = 2r^2/k$ and $\alpha = -8n/k$ in Eq. (38), we have

$$tF_t'' + \left(n - \frac{t}{4}\right)F_t = 0 \tag{39}$$

Further, let $F_t = E_t(t/2)e^{-t/2}$. Then Eq. (39) becomes

$$tE'' + (2-t)E' + (n-1)E = 0 \tag{40}$$

Equation (40) is a standard Laguerre associated differential equation. The solutions of Eq. (40) are given by the associated Laguerre polynomials (Ref. [10], pp. 155–156). By means of backward substitutions, we obtain

$$F_n = L_n^1\left(\frac{2r^2}{k}\right)\frac{r^2}{k}e^{-r^2/k} \quad \text{for } \alpha = -\frac{8n}{k} \quad n = 1,2,3,\ldots \tag{41}$$

Substituting this into Eq. (37) yields

$$G_n = a_n e^{-\sqrt{8n/k}z} + b_n e^{\sqrt{8n/k}z} \tag{42}$$

G_n must be a bounded function so that b_n is equal to zero. Combining Eqs. (28), (41), and (42), a complete solution in the form of a series of associated Laguerre polynomials Eq. (22) is obtained (in that equation, $c_n = a_n/k$).

Boundary conditions (9), (11), and (12) are satisfied automatically. For the wall boundary condition (Eq. (10)), setting $z=0$ in Eq. (22), multiplying by $e^{-r2/k}L_m^1(2r^2/k)$, then integrating from $r=0$ to ∞, the orthogonality of Laguerre polynomials leads to a set of equations and yields the coefficients c_n (Eq. (23)).

Finally, substituting Eq. (22) into Eq. (4) yields the radial and axial velocities (Eqs. (24) and (25)), as we claimed.

Setting $k=1$, Eq. (22) becomes the simple Gaussian impinging jet solution obtained by Lee et al. [6], which is a particular case in the solution family. Note that their expression for coefficients $c_n = (-1)^n/(n+1)$ is not correct (most likely a print error), conducting to a divergent solution.

2.4 Analytical Solutions for Plane Impinging Jets. For the plane impinging jets, a solution similar to Eq. (22) exists as well. A simpler analytical solution is found and presented herein:

(a) Stream function:

$$\psi = \frac{1}{k}[k-(k+x)e^{-2x/k}][(k+z)e^{-2z/k}-k] \tag{43}$$

It is easy to see that $\psi \sim xz$ as x and z are small.

(b) Velocity in the x direction:

$$u(x,z) = \left[1-\left(1+\frac{x}{k}\right)e^{-2x/k}\right]\left(1+\frac{2z}{k}\right)e^{-2z/k} \tag{44}$$

(c) Velocity in the z direction:

$$w(x,z) = \left[\left(1+\frac{z}{k}\right)e^{-2z/k}-1\right]\left(1+\frac{2x}{k}\right)e^{-2x/k} \tag{45}$$

For the particular cases of the impinging plate surface and the jet centerline, we have the associated velocities expressed as

$$u(x,0) = 1-\left(1+\frac{x}{k}\right)e^{-2x/k} \tag{46}$$

$$w(0,z) = \left(1+\frac{z}{k}\right)e^{-2z/k}-1 \tag{47}$$

Derivation. Let $\psi = CX(x)\cdot Z(z)$. Then integrating Eq. (20) from 0 to x, we obtain

$$X(x) = X_{z=\infty} = \int_0^x w dx = k-(k+x)e^{-2x/k} \tag{48}$$

Due to symmetry,

$$Z(z) = Z_{x=\infty} = -\int_0^z u dz = (k+z)e^{-2z/k}-k \tag{49}$$

Substituting the above results into the stream function, we obtain

$$\psi = C[k-(k+x)e^{-2x/k}][(k+z)e^{-2z/k}-k] \tag{50}$$

Note that the velocity at the infinite centerline should reach unity, i.e.,

$$-w(z=\infty, x=0) = 1 \tag{51}$$

This leads to $C = 1/k$, and Eq. (43) is obtained.

The above solution can be verified to satisfy both the differential equations (6)–(8) and the boundary conditions (13)–(15) by direct substitution.

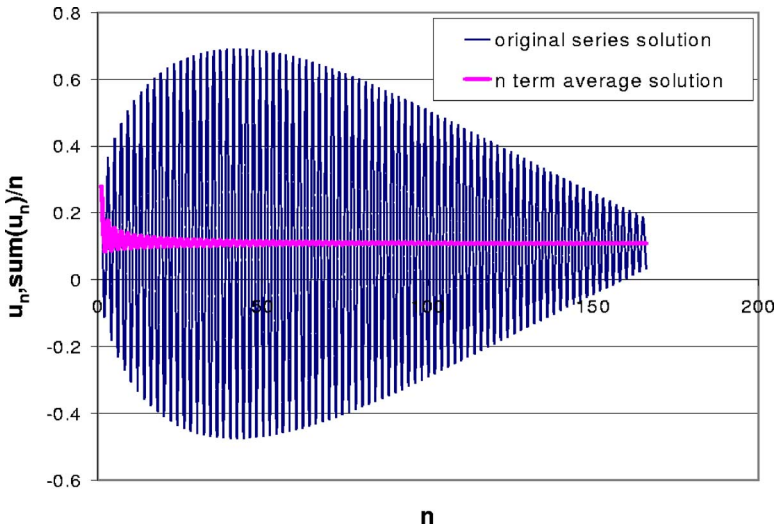

Fig. 1 Comparison of front *n* term average value series

3 Implementation for Round Impinging Jets

It is necessary to develop a method to obtain a stable convergent result for the flow field parameters from Eqs. (22), (24), and (25), because all of the parameters are expressed by oscillatory series. A front n term averaged method is put forward and found efficient for the flow field computations. The method is based on the following theorem.

THEOREM. For a given convergent oscillatory series, the average values of the first n terms constitute a series that will converge to the same value as that of the original series and the first n term average value series has a faster convergence speed.

The detailed proof of the above theorem is given in the Appendix.

Lee et al. [6] showed that the solution of a simple Gaussian impinging jet converges with terms decaying as $n^{-1/4}$. The present method produces a much faster converging rate of n^{-1}. For example, if we search for solutions of accuracy of 1%, we need 10^8 terms in the original series while we need 100 terms only in the front n term average series. Moreover, as it will be demonstrated later, even if the original series is not convergent, the average value series can still provide a "convergent value."

Figure 1 illustrates this method with a comparison between the original velocity series solution and its front n term average value solution. Accordingly, the maximum relative error of the front n term average value series is less than $1/n$.

Fortunately, all parameters, including the average value series, can be expressed by recurrence formulas, which allow us to obtain the desired accuracy. Here are the recurrence formulas used in the implementation (Eq. (53) can be found in a mathematical handbook, see Ref. [9], p. 156):

$$c_{n+1} = -c_n \frac{n}{(n+1)^2} \tag{52}$$

$$L_1^1 = -1 \quad L_2^1 = 2\left(\frac{2r^2}{k} - 2\right)$$

$$L_n^1 = \frac{n}{n-1}\left\{\left[2(n-1) - \frac{2r^2}{k}\right]L_{n-1}^1 - (n-1)^2 L_{n-2}^1\right\} \quad n = 3,4,\ldots \tag{53}$$

$$\frac{\partial L_1^1}{\partial r} = 0 \quad \frac{\partial L_2^1}{\partial r} = \frac{8r}{k}$$

$$\frac{\partial L_n^1}{\partial r} = \frac{n}{n-1}\left\{\left[2(n-1) - \frac{2r^2}{k}\right]\frac{\partial L_{n-1}^1}{\partial r} - (n-1)^2\frac{\partial L_{n-2}^1}{\partial r}\right\} - \frac{4nr}{(n-1)k}L_{n-1}^1 \quad n = 3,4,\ldots \tag{54}$$

The origin $O(0,0)$ is a singular point for Eq. (3). The solution displays this feature from Eq. (27), since the axial velocity is not convergent at the origin:

$$w(0,\,0) = -1 + 2 - 2 + \cdots, \quad \text{i.e.,} \quad w_1(0,\,0) = 1 \quad w_2(0,\,0) = -1, \ldots \quad w_n(0,\,0) = (-1)^{n-1} \tag{55}$$

With the aid of the front n term averaged method, a convergent value $w(0,0)=0$ is obtained, which is its physical velocity value.

For any other points in the domain, stable convergent flow field parameters can be obtained using the above method.

4 Boundary Layer Approximation

Comparing the solution of plane stagnation point flow and that of axial-symmetric stagnation flow (Ref. [10], pp. 152–159), one can see that the boundary layer thickness of a plane stagnation flow is 1.2 times of that of the axial symmetric:

$$\delta^*_{\text{plane}} = 1.2\delta^*_{\text{asym}} \tag{56}$$

The above expression can be used to determine the boundary layer depth for plane jet impingement as long as the boundary layer depth for the round jet case has been determined or vice versa.

Based on impinging jet experiments [7], the following empirical expressions were obtained to describe the dimensionless boundary layer depth for the round impinging jet:

$$\delta = \frac{4.5}{\sqrt{\text{Re}_j}}\sqrt{\frac{r}{u_s}} \quad \text{for local } \text{Re}_l < 2.5 \times 10^4 \tag{57}$$

$$\frac{\sqrt{r}}{\sqrt{\delta}} = -1.95\ln\left(\frac{\Delta}{0.16R^*} + \frac{278}{\text{Re}_j u_s r\sqrt{\delta}}\right) \quad \text{for } \text{Re}_l > 2.5 \times 10^5 \tag{58}$$

where Re_j is the jet Reynolds number, $\text{Re}_j = w^*_{\text{jet}} R^*/2\nu$; Re_l is the local Reynolds number, $\text{Re}_l = u^*_s r^*/\nu$; Δ is the roughness height (in m); ν is the kinematical viscosity (in m^2/s); u^*_s is the inviscid surface velocity (in m/s).

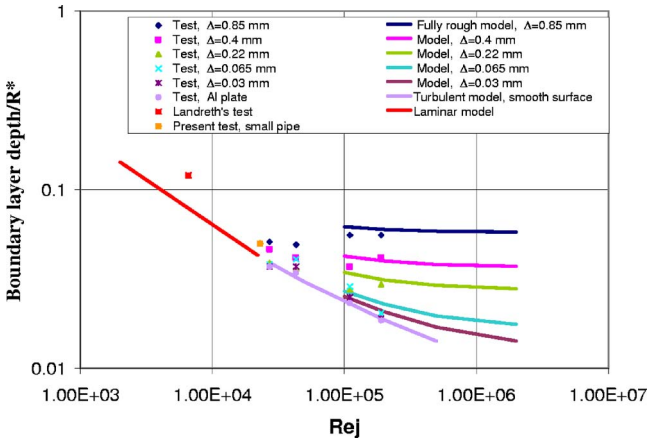

Fig. 2 Comparison of the impinging jet boundary layer depths between empirical models and roughness test data (Δ is the roughness height of the sandpaper)

Note that r, δ, and u_s above are dimensionless variables.

Figure 2 shows a comparison of the empirical expressions (57) and (58) with the boundary layer depth experimental data. When the Reynolds number is less than a critical value ($\mathrm{Re}_j \approx 2.5 \times 10^4$), the flow is Reynolds number dependent. Above one order of the critical value, an asymptotic state is reached where the boundary layer increases with the surface roughness.

The displacement depths can be estimated by (Ref. [11], pp. 30–36)

$$\delta_{\mathrm{disp}} = \delta/3 \quad \text{for a laminar flat plate boundary layer} \tag{59}$$

and

$$\delta_{\mathrm{disp}} = \delta/7 \quad \text{for a turbulent flat plate boundary layer} \tag{60}$$

The radial velocity profiles of the impinging jet for the combined model (inviscid solution plus the boundary layer approximation) are presented in the following two subsections.

4.1 Laminar Boundary Layer Case. We divide the z domain into three regions ($[0 \sim \delta]$, $[\delta \sim 4\delta/3]$, and $[4\delta/3 \sim \infty]$) and obtain the combined velocity profiles by the following steps:

(a) We displace the inviscid velocity profile up a distance of δ_{disp} from the ground surface.

(b) In the outer region, we use the displaced inviscid velocity profile:

$$u(r,z) \Leftarrow u(r, z - \delta/3) \quad \text{for } z \geqslant 4\delta/3 \tag{61}$$

(c) In the region of $z=[\delta \sim 4\delta/3]$, we use a parabolic equation to smooth the curve to the maximum value of u. The parabolic equation is subjected to the following three constraints:

$$u(r,\ 4\delta/3) \Leftarrow u(r,\ \delta) \quad \partial u/\partial z(r,\ 4\delta/3) \Leftarrow \partial u/\partial z(r,\ \delta)$$
$$\partial u/\partial z(r,\ \delta) = 0 \tag{62}$$

This yields

$$u(r,z) = A_1 z^2 + B_1 z + C_1 \tag{63}$$

with

$$A_1 = \frac{3u_z'(r,\ \delta)}{2\delta} \quad B_1 = -3u_z'(r,\ \delta)$$
$$C_1 = u(r,\delta) + \frac{4}{3}\delta u_z'(r,\ \delta) \tag{64}$$

and the maximum velocity

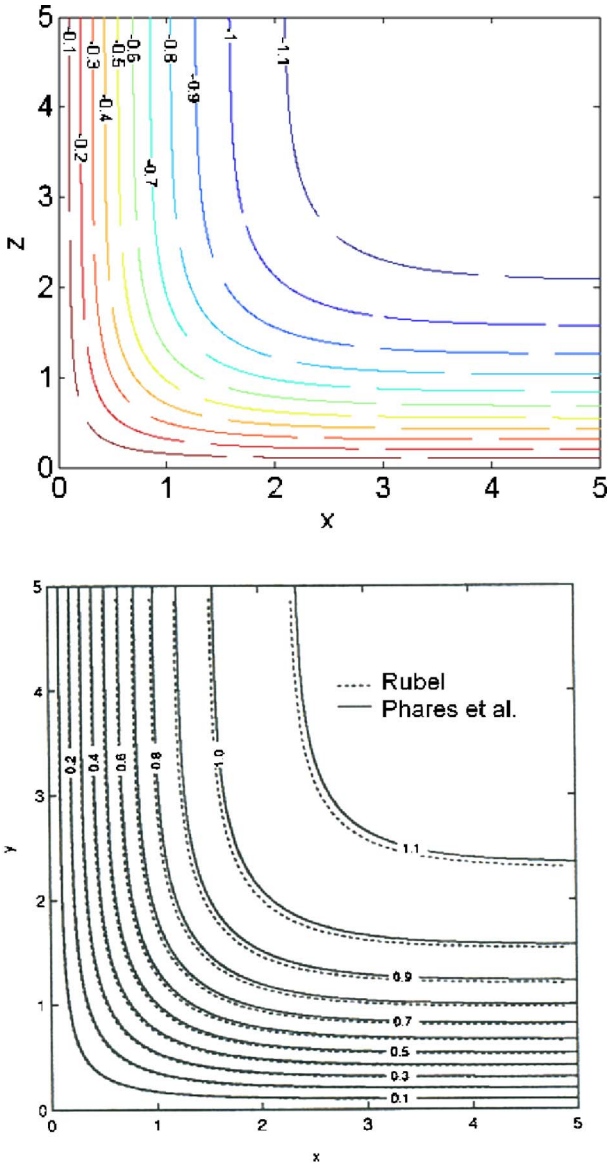

Fig. 3 Streamlines of a plane impinging jet model: (*a*) present model (−ψ corresponds to Rubel's ψ value); (*b*) calculated by Rubel and Phares et al., cited from Ref. [5]

$$u_{\max}(r,\delta) = u(r,\delta) - \frac{1}{6}\delta u_z'(r,\delta) \approx \frac{1}{2}\left[u\left(r,\ \frac{2}{3}\delta\right) + u(r,\delta)\right] \tag{65}$$

where

$$u_z'(r,z) = -re^{-r^2/k}\sum_{n=1}^{\infty} c_n \frac{8n}{k} L_n^1\left(\frac{2r^2}{k}\right) e^{-(\sqrt{8n/k})z} \tag{66}$$

(d) Within the boundary layer ($z < \delta$), we use the polynomial approximation of Homman's boundary layer velocity profile (data from Ref. [10], p. 156, Tables 3–4):

$$u(r,\eta) = (-1.43\eta^4 + 5.39\eta^3 - 7.45\eta^2 + 4.49\eta)u_{\max}(r,\delta) \quad \text{for } \eta \leqslant 1 \tag{67}$$

where $\eta = z/\delta$.

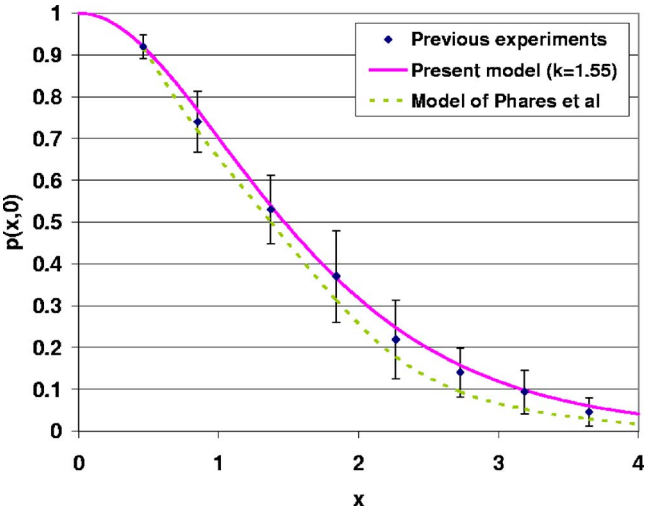

Fig. 4 Comparison of surface pressure distribution (the error bar is for the experiments)

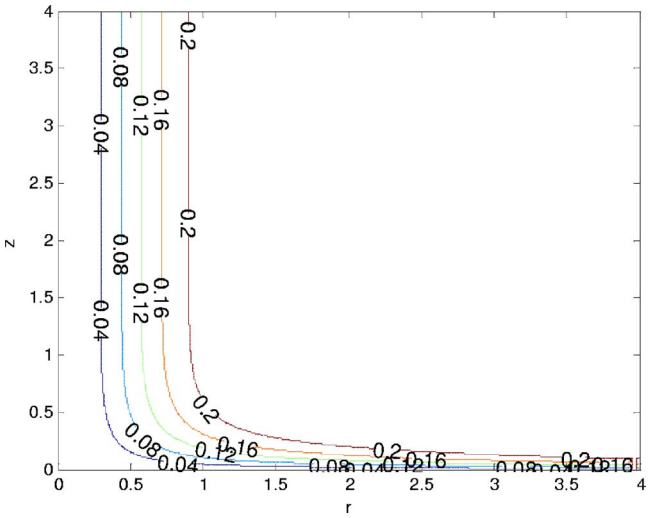

Fig. 5 Laminar circular impinging jet streamlines ($-\psi$ is used)

4.2 Turbulent Boundary Layer Case. Similar to the laminar case, we divide the z domain into three parts ($[0 \sim \delta]$, $[\delta \sim 8\delta/7]$ and $[8\delta/7 \sim \infty]$) and obtain the radial velocity profiles by the following steps:

(a) We displace the inviscid velocity profile up a distance of δ_{disp} from the ground surface.

(b) In the outer region, $z=[8\delta/7 \sim \infty]$, we use the displaced inviscid velocity profile:

$$u(r,z) \Leftarrow u(r,z-\delta/7) \quad \text{for } 8\delta/7 \leqslant z \tag{68}$$

(c) In the region of $z=[\delta \sim 8\delta/7]$, we use a parabolic equation to smooth the curve to the maximum value of u. The parabolic equation is subjected to the following three constraints:

$$u(r,\ 8\delta/7) \Leftarrow u(r,\delta) \quad \partial u/\partial z(r,\ 8\delta/7) \Leftarrow \partial u/\partial z(r,\delta)$$

$$\partial u/\partial z(r,\delta) = 0 \tag{69}$$

This yields

$$u(r,z) = A_2 z^2 + B_2 z + C_2 \tag{70}$$

with

$$A_2 = 7u_z'(r,\delta)/2\delta \quad B_2 = -7u_z'(r,\delta)$$

$$C_2 = u(r,\delta) + \frac{24}{7}\delta u_z'(r,\delta) \tag{71}$$

and the maximum velocity

$$u_{\max}(r,\delta) = u(r,\delta) - \frac{1}{14}\delta u_z'(r,\delta) \approx \frac{1}{2}\left[u\left(r,\ \frac{6}{7}\delta\right) + u(r,\delta)\right] \tag{72}$$

(d) Within the boundary layer ($z \leqslant \delta$), we use Eq. (67) or any similar expressions for turbulent boundary layers.

5 Results and Comparisons

Example 1. Plane impinging jets. Equation (27) can be used to calculate the values of stream functions with different k. Figure 3(*a*) is an example of the mapped streamlines in a 5×5 domain (set $k=1.16$), which matches the numerical and analytical-numerical mixed results, see Fig. 3(*b*), cited from Ref. [5].

According to the definition (see Eq. (2)), the normalized pressures on the surface of the impinging jet plate can be determined from Bernoulli's equation, i.e.,

$$p(x,\ 0) = 1 - u^2(x,\ 0) \tag{73}$$

where $u(x,0)$ is the surface radial velocity from the inviscid model.

Phares et al. [5] compared the surface pressure distribution for a plane impinging jet with previous experiments including these

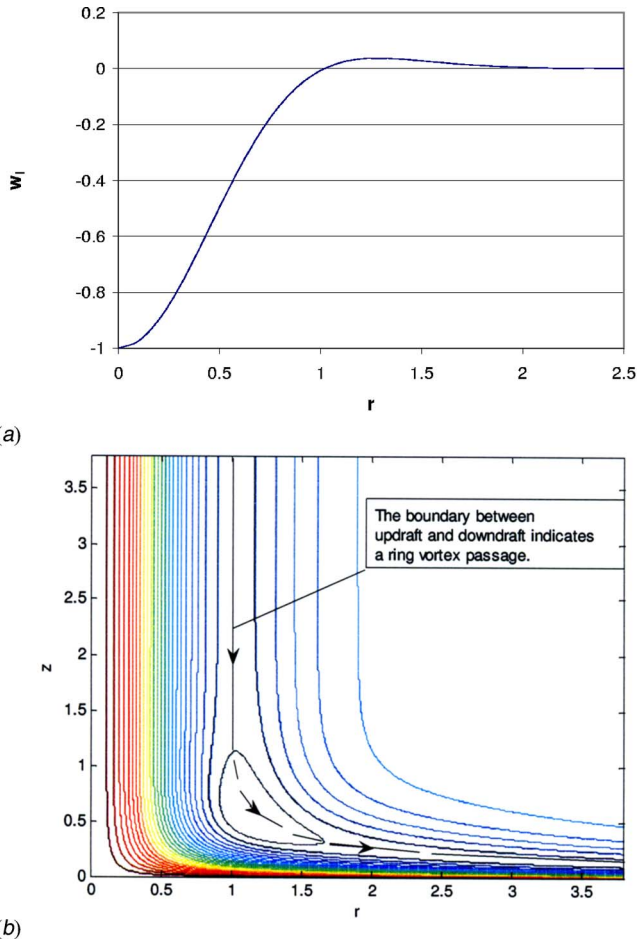

Fig. 6 An axis symmetric impinging jet combined model with updraft and downdraft: (*a*) influx profile; (*b*) contours of stream function

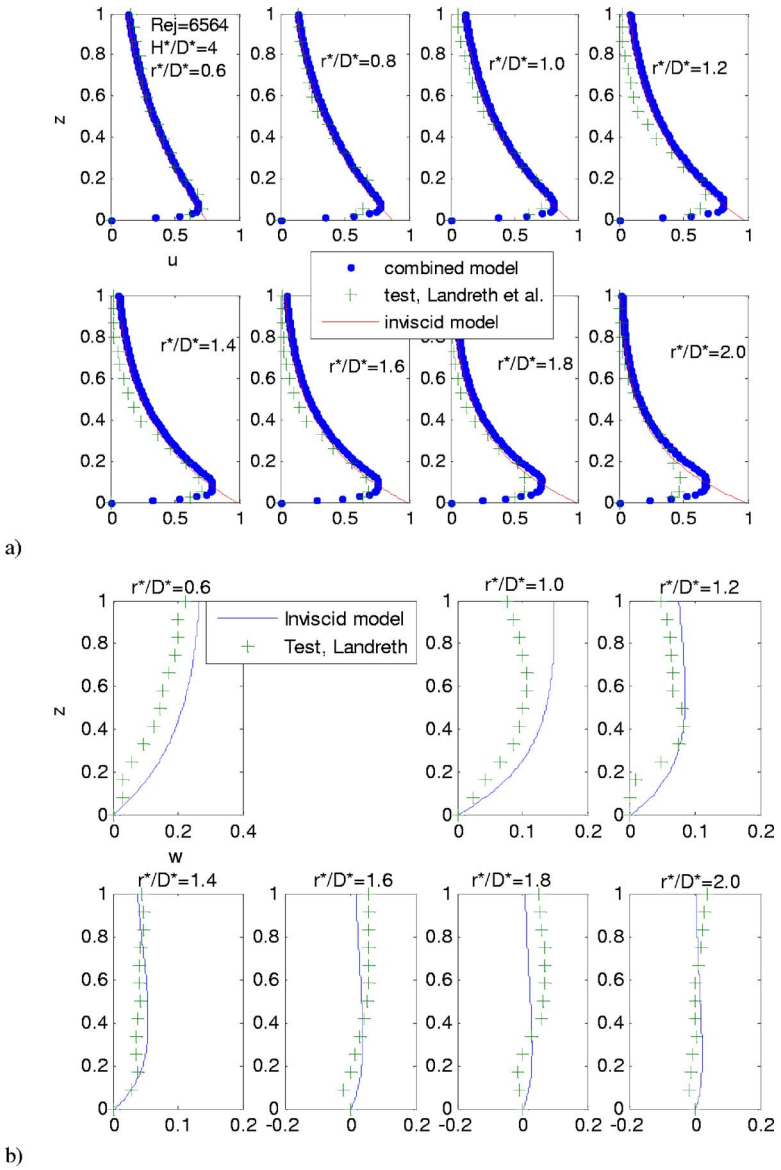

Fig. 7 Velocity comparison (model: $k=2.05$; test: $H^*/D^*=4$, cited from Ref. [17]): (*a*) radial velocity profiles; (*b*) axial velocity profiles

by Kumada and Mabuchi [12], and Beltaos and Rajaratnam [13]. The present model shows improved fitting of the experimental data (see Fig. 4). In Fig. 4, $k=1.55$ is chosen for the present model according to the fully developed jet condition of $H^*/B_0^*=12$.

Example 2. Axis symmetric impinging jets.

(*a*) *Streamlines for a laminar axis symmetric impinging jet.* For a laminar flow in a circular pipe (Hagen-Poiseuille flow), the velocity profile is parabolic about the centerline, and the average velocity is equal to half of the centerline velocity (Ref. [11], p. 116):

$$\bar{u}=\frac{1}{2}u_{\max} \tag{74}$$

where $u_{\max}$ is the centerline velocity. Hence, $k=1/2$ is chosen to model the laminar impinging jet, i.e., the influx velocity into the domain at $z=\infty$ is

$$w_\infty=-e^{-2r^2} \quad \text{and} \quad \psi_\infty=-\frac{1}{4}(1-e^{-2r^2}) \tag{75}$$

Figure 5 shows the streamlines of the laminar impinging Gaussian jet based on the analytical model.

(*b*) *Vortex trace for a turbulent axis symmetric impinging jet.* The trace of vortices in the mixing layer of a turbulent impinging jet is determined using the analytical model. In order to generate a vortex trace using this inviscid model, a mixed influx velocity profile is used with both down flow and up flow in conjunction with the inviscid model. The boundary between the two opposite direction velocities can be considered the trace of the ring vortices. The following influx velocity function has the mixed shape with a velocity value of 0 at $r\approx 1$:

$$w_\infty=-2e^{-2r^2}+e^{-4r^2/3} \tag{76}$$

This combined influx velocity profile, shown in Fig. 6(*a*), corresponds to twice a downdraft of $k=0.5$ and an updraft of $k=0.75$.

The stream function is now expressed by $2\psi(0.5)-\psi(0.75)$, where $\psi(k)$ is defined by Eq. (22). The corresponding streamlines are shown in Fig. 6(*b*).

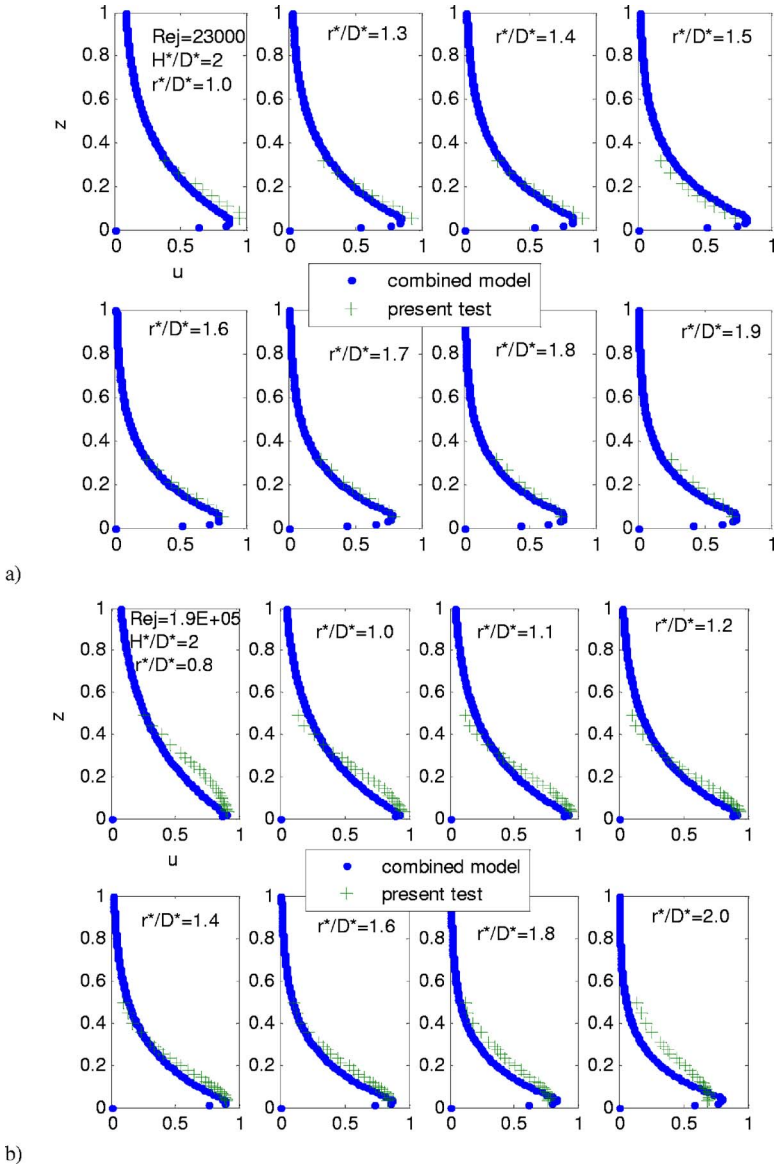

Fig. 8 Radial velocity comparisons for turbulent circular impinging jets: (*a*) $Re_j=23000$, $H^*/D^*=2$; (*b*) $Re_j=190000$, $H^*/D^*=2$.

(*c*) *Velocity field of experimental axis symmetric impinging jets*. In order to compare the combined model with experiments, the parameter k is determined according to the particular test conditions. Landreth and Adrian [14] presented the velocity profiles of a turbulent circular jet based on PIV measurements ($D^*=26.9$ mm, $H^*/D^*=4$, $Re_j=6564$, fluid: water). Substituting $H^*/R^*=2H^*/D^*=8$ into Eq. (15), the parameter k is obtained as

$$k = 2.2(0.08 \times 8 + 0.294) = 2.05 \tag{77}$$

Therefore, the flow parameters of a Gaussian impinging jet of $k=2.05$ are computed and compared with Landreth and Adrian's experiments.

Figure 7(*a*) compares the radial velocity profiles for the $H^*/D^*=4$ case. The inviscid model is modified with a laminar boundary layer approximation described in Sec. 4.1. It is shown that the model compares well against the experiments. Figure 7(*b*) compares the axial velocity profiles for the same case. It can be observed that for r^*/D^* in [0.8, 1.4], the model and experimental profiles are consistent. For $r^*/D^*>1.6$, some negative axial velocity values are observed in the near surface experimental results that are not reproduced by the model.

Figure 8(*a*) compares the radial velocity profiles for another case. The experimental results are from measurements taken with a boundary layer probe in a small impinging jet facility [7] and correspond to $H^*/D^*=2$ and $Re_j=23{,}000$. Again, the inviscid model is modified with a laminar boundary layer approximation and shows good agreement with the experiments.

Figure 8(*b*) compares the radial velocity profiles from a larger jet facility test for $H^*/D^*=2$ and $Re_j=190{,}000$ [7]. Here, the inviscid model is modified with a turbulent boundary layer approximation described in Sec. 4.2. While, overall, the model agreement with the test data is fair, note the difficulty in reproducing the thinner surface layer at this higher Reynolds number, see also Fig. 2.

(*d*) *Surface pressures of turbulent axis symmetric impinging jets*. For axis symmetric impinging jet cases, the normalized pressures on the surface of the impinging jet plate can be expressed by

$$p(r,\ 0) = 1 - u^2(r,\ 0) \tag{78}$$

where $u(r,0)$ is the surface radial velocity from the inviscid model.

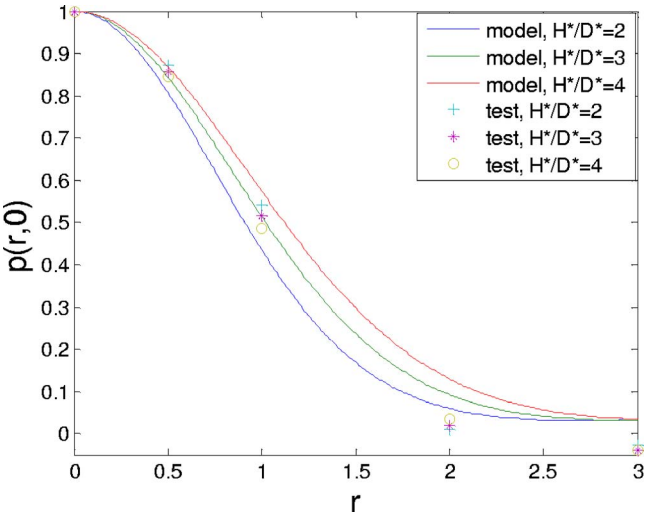

Fig. 9 Comparison of the plate surface pressure distribution

Pressure tests were carried out with a small impinging jet facility ($D^*=38$ mm, $\mathrm{Re}_j=23{,}000$) [7] and compared here with the model predictions in Fig. 9. While the model shows a more pronounced sensitivity to H^*/D^* compared to the experiments, the overall agreement with the experiments is quite good.

Example 3: Annular influx impinging jets. In order to model an annular jet impingement, the influx velocity profile can be expressed by multiple Gaussian jet equations, namely, by

$$-w_\infty = a_3 e^{-r^2/K_1} - b_3 e^{-r^2/K_2} \tag{79}$$

For a certain influx velocity profile, the radius corresponding to the maximum velocity (r_m) and the maximum deficit velocity ($\delta w = w_\infty(r_m) - w_\infty(0)$) are usually specified. Subject to the constrains of $w_\infty(r_m)=-1$ and $dw_\infty/dr|_{r=rm}=0$, the parameters in Eq. (79) can be found by solving the following iterations:

$$K_1 = tr_m \quad K_2 = tr_m/2$$

$$t = \frac{r_m}{\ln(2b_3/a_3)} \quad a_3 = \frac{1-\delta w - e^{2r_m/t}}{1-e^{r_m/t}} \quad b_3 = a_3 + \delta w - 1 \tag{80}$$

For example, if $\delta w=0.8$ and $r_m=0.65$ are set, the following expression based on Eqs. (79) and (80) is found:

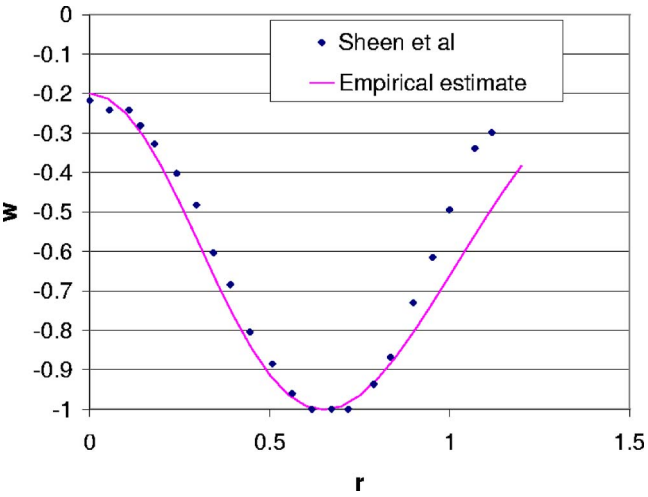

Fig. 10 Particular influx velocity profile of an annular jet

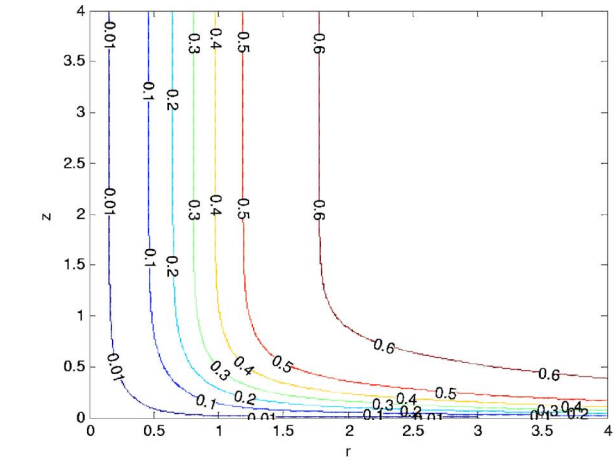

a)

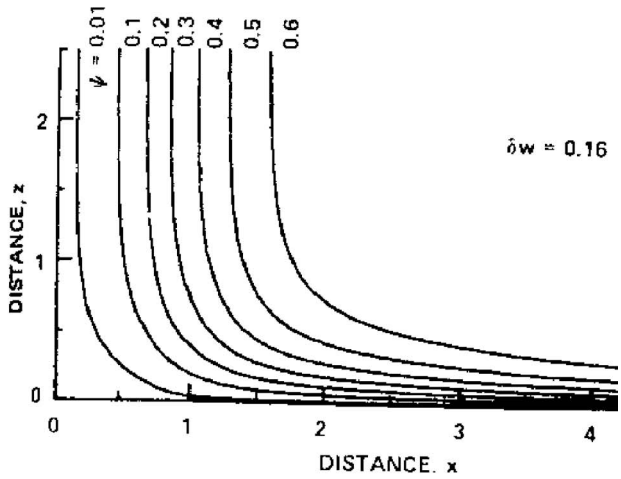

b)

Fig. 11 Annular impinging jet ($r_m=0.35$, $\delta w=0.16$): (*a*) streamlines by present model ($-\psi$ is used); (b) numerical solution by Rubel [16]

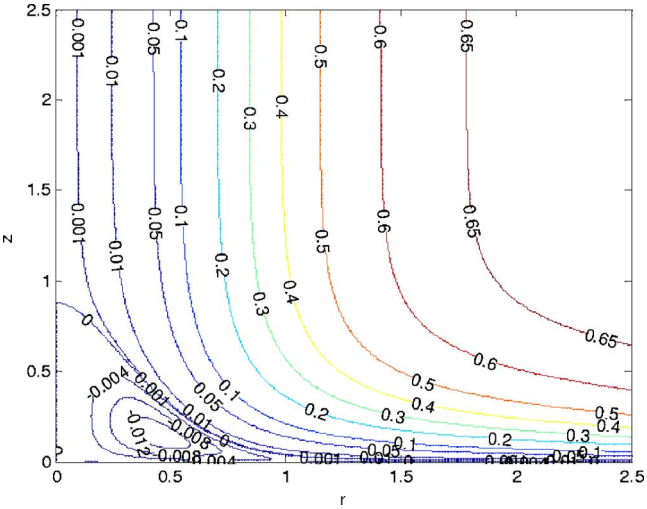

Fig. 12 Streamlines for an annular impinging jet with the influx profile shown in Fig. 10 ($r_m=0.65$, $\delta w=0.8$)

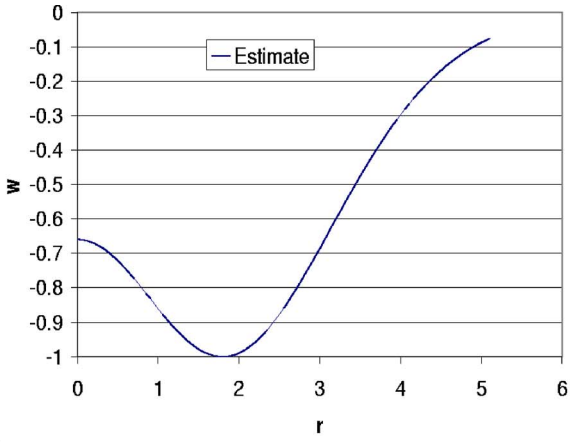

a)

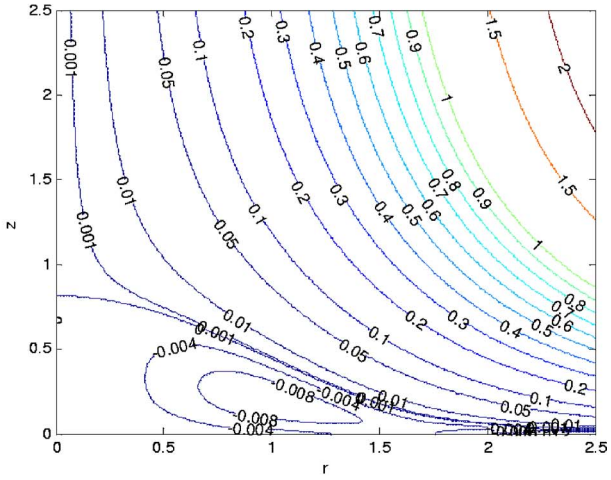

b)

Fig. 13 An annular impinging jet with a large recirculation ring: (*a*) influx velocity profile estimated from the surface pressure values of Ref. [8]; (*b*) Streamlines (−ψ is used)

$$-w_\infty = 3.79e^{-r^2/0.661} - 3.59e^{-r^2/0.330} \tag{81}$$

This particular expression provides reasonable agreement with the experimental data by Sheen et al. [15], see Fig. 10.

The two terms of Eq. (81) are used to form two Gaussian impinging jet stream functions ($K_1=0.661$, $K_2=0.33$), which, when added together, provide the stream function

$$\psi = 3.59\psi(0.33) - 3.79\psi(0.661) \tag{82}$$

where $\psi(k)$ is expressed by Eq. (22).

(*a*) *Comparison with previous numerical and mixed models*. The present model is in good agreement with the numerical flow field simulated by Rubel [16] for $r_m=0.35$, $\delta w=0.16$, and $\Omega(0)=0$. In this case, no flow recirculation zone appears, see Fig. 11. The recirculation zone is predicted by Rubel's numerical model only when a nonzero value of $\Omega(0)$ is specified [16]. The present model can also predict a recirculation zone when δw exceeds 0.2 (even up to the maximum 1), in which case, Rubel's method becomes divergent.

Figure 12 shows the contours of the stream function of the annular impinging jet for $r_m=0.65$ and $\delta w=0.8$, which are in good agreement with the analytical-numerical mixed solution by Phares et al. [5]. For this case, Rubel's model [16] has no convergent solution.

(*b*) *Comparison with the experiment by Donaldson and Snedeker*. Figure 13(*a*) shows another influx profile estimated from the Bernoulli equation using the experimental impinging plate surface pressures by Donaldson and Snedeker [17]. Figure 13(*b*) shows the streamlines generated by the present model using the estimated influx profile. The model predicts a stagnation bubble with the radius comparable to the experiments.

6 Concluding Remarks

An inviscid solution for a family of Gaussian orthogonal impinging jets is derived and it constitutes a base for analytical modeling of the flow field of various real impinging jets. The solution is robust and extends the analytical model by Lee et al. [6]. A first n term averaged method is put forward to speed up the convergence of the oscillatory series, thus simplifying the flow field computations. A new and simpler solution of the plane impinging jets is also obtained.

The inviscid solutions are then combined with laminar and turbulent boundary layer solutions to model real impinging jets. This family of combined inviscid-boundary layer solutions compare well in terms of flow field (streamlines, ring vortex trace, and velocities) and surface pressure field with experiments for both laminar and turbulent boundary layers and different Reynolds numbers. Moreover, an expression for an annular jet profile is derived. The solutions of several annular impinging jets show good agreement with numerical, mixed models, and experimental results.

Acknowledgment

This work was made possible through funding provided by Natural Science and Environmental Research of Canada (NSERC) Grant No. 166732 and funding from Manitoba Hydro. Thanks are also due to Dr. David Surry for providing many valuable suggestions.

Nomenclature

a_1, a_2 = jet shape coefficients
b_1, b_2 = empirical constants
B_0^* = half-width of plane jet slot, m
D^* = diameter of round jet, m
H^* = distance between jet outlet and impinging plate, m
k = flow rate multiplier
p^* = pressure, Pa
p = dimensionless pressure, $p=2p^*/\rho w_m^2$
Q = dimensionless flow rate
R^* = radius of round jet, m
Re_j = Reynolds number of jet flow based on jet diameter D^* and jet velocity w_m
Re_l = local Reynolds number based on radial distance r^* and surface velocity u_s^*
r^*, z^* = radial and axial coordinates, m
r, z = dimensionless radial and axial coordinates; $r=r^*/R^*$, $z=z^*/R^*$
u^*, w^* = radial and axial velocities, m/s
u_s^* = inviscid velocity on impinging plate surface, m/s
u, w = dimensionless radial and axial velocities, $u=u^*/w_m$, $w=w^*/w_m$
r_m = radius corresponding to maximum velocity
w_m = maximum axial velocities at jet center line, m/s
δw = maximum deficit velocity
x, z = dimensionless plane coordinates; $x=x^*/B_0^*$, $z=z^*/B_0^*$

Greek Symbols

ρ = fluid density, $\mathrm{kg/m^3}$
ν = kinematical viscosity, $\mathrm{m^2/s}$
Δ = roughness height of sand paper grain, m

δ^* = thickness of viscous boundary layer, m
δ = dimensionless thickness of viscous boundary layer
δ^*_{disp} = displacement thickness of viscous boundary layer, m
δ_{disp} = dimensionless displacement thickness
ψ = stream function
Ω = vorticity function

Appendix: Proof of Convergence of the Front *n* Term Average Value Series

Given a series $\Sigma_{i=1}^{\infty} a_i$, let the partial summation of the series be a sequence:

$$S_n = \sum_{i=1}^{n} a_i \quad n = 1,2,\ldots \tag{A1}$$

Then take the average of S_n as a new sequence:

$$\bar{S}_n = \frac{1}{n}\sum_{i=1}^{n} S_i \quad n = 1,2,\ldots \tag{A2}$$

We want to prove that

(i) if $\lim_{n\to\infty} S_n = S$, then $\lim_{n\to\infty} \bar{S}_n = S$;
(ii) if further $S_i S_{i+1} < 0$, $i = 1,2,\ldots$, then $\text{cov}\,\bar{S}_n > \text{cov}\,S_n$.

(Here, cov denotes the rate of convergence.)

Proof. To prove (i), we need to show that

For any $\varepsilon > 0$, there exists an integer N' such that $|\bar{S}_n - S| < \varepsilon \; \forall n > N'$.

From $\lim_{n\to\infty} S_n = S$, we know that the sequence is bounded, i.e.,

$$|S_n - S| \leqslant M \quad \forall\, n = 1,2,\ldots,(M > 0) \tag{A3}$$

Also, since $\lim_{n\to\infty} S_n = S$, for any chosen $\varepsilon > 0$, we can find an integer N such that

$$|S_n - S| < \frac{1}{2}\varepsilon \quad \forall\, n > N \tag{A4}$$

Then, for $n > N$,

$$\begin{aligned}
|\bar{S}_n - S| &= \left|\frac{1}{n}\sum_{i=1}^{n} S_i - S\right| \\
&= \frac{1}{n}|S_1 + S_2 + \cdots + S_n - nS| \\
&= \frac{1}{n}|(S_1 - S) + (S_2 - S) + \cdots + (S_n - S)| \\
&\leqslant \frac{1}{n}(|S_1 - S| + |S_2 - S| + \cdots + |S_n - S|) \\
&= \frac{1}{n}(|S_1 - S| + |S_2 - S| + \cdots + |S_N - S| + |S_{N+1} - S| \\
&\quad + \cdots + |S_n - S|) \\
&\leqslant \frac{1}{n}\left[NM + \frac{1}{2}(n - N)\varepsilon\right] \quad \text{(Eqs.(A3) and (A4) are used)} \\
&= \frac{NM}{n} + \frac{n - N}{2n}\varepsilon < \frac{NM}{n} + \frac{1}{2}\varepsilon
\end{aligned} \tag{A5}$$

Now, let

$$N' = \left(\frac{2NM}{\varepsilon}\right) + 1 \tag{A6}$$

where the notation [ ] represents the largest integer $\leqslant 2NM/\varepsilon$. Then, it follows from Eq. (A5) that for $n > N'$,

$$|\bar{S}_n - S| < \frac{NM}{n} + \frac{1}{2}\varepsilon < \frac{NM}{N'} + \frac{1}{2}\varepsilon < \frac{NM}{2NM/\varepsilon} = \frac{1}{2}\varepsilon + \frac{1}{2}\varepsilon = \varepsilon \tag{A7}$$

This proves Part (i).

Note that for Part (i), the reverse is not true, i.e., if $\lim_{n\to\infty} \bar{S}_n = S$, it is not necessary to have $\lim_{n\to\infty} S_n = S$. For example, consider the sequence of $S_1 = -0.1$, $S_n = 0.4 + (-1)^n$ for $n \geqslant 2$: $-0.1, 1.4, -0.6, 1.4, \ldots, 0.4 + (-1)^n, \ldots$. It is easy to see that

$$\bar{S}_n = \frac{1}{n}\sum_{i=1}^{n} S_i = 0.4 \pm \frac{1}{2n} \to 0.4 \quad \text{as } n \to \infty$$

However, S_n is not convergent.

The above counterexample implies that the rate of convergence of the sequence $\bar{S}_n$ is greater than that of the sequence S_n if S_n is randomly alternating between $+M_1$ and $-M_2$ (M_1, M_2 are positive bounded numbers). It also shows that, conservatively, the rate of convergence of the sequence $\bar{S}_n$ is proportional to n^{-1} (the above counter example is the worst case whose terms reach the two bounded numbers for all $n \geqslant 2$). However, it is not easy to prove this in general. In the following, we prove Part (ii) under the assumption that S_n is an alternative sequence about its limit, i. e., $(S_n - S)(S_{n+1} - S) < 0$.

Without loss of generality, suppose S_n changes sign from $n = 1$ and $|S_n - S|$ is decreasing. Then, it is easy to prove that $\bar{S}_n$ is also an alternative sequence. Further, suppose $S_n - S > 0$ and $S_{n+1} - S < 0$. Similarly, we have $\bar{S}_n - S > 0$, and $\bar{S}_{n+1} - S < 0$. Assume that $S > 0$ (if $S < 0$, we can consider the sequence $-S_n$ and the same argument applies). Then,

$$|S_n - S| - |S_{n+1} - S| = S_n + S_{n+1} - 2S > 0 \Rightarrow S_n + S_{n+1} > 0 \tag{A8}$$

and

$$|\bar{S}_n - S| - |\bar{S}_{n+1} - S| = \bar{S}_n + \bar{S}_{n+1} - 2S > 0 \Rightarrow \bar{S}_n + \bar{S}_{n+1} > 0 \tag{A9}$$

We want to prove that there exists $\bar{N}$ such that

$$\begin{aligned}
F(\bar{S}_n, \bar{S}_{n+1}, S) &\equiv |\bar{S}_n - S| - |\bar{S}_{n+1} - S| < |S_n - S| - |S_{n+1} - S| \\
&\equiv F(S_n, S_{n+1}, S)
\end{aligned} \tag{A10}$$

A direct calculation shows that

$$\begin{aligned}
&F(\bar{S}_n, \bar{S}_{n+1}, S) \\
&\quad = |\bar{S}_n - S| - |\bar{S}_{n+1} - S| = \bar{S}_n - S + \bar{S}_{n+1} - S \\
&\quad = \frac{1}{n}(S_1 + S_2 + \cdots + S_n) - S \\
&\quad + \frac{1}{n+1}(S_1 + S_2 + \cdots + S_n + S_{n+1}) - S \\
&\quad = \frac{1}{n}[(S_1 - S) + (S_2 - S) + \cdots + S_{n-1} - S)] + \frac{1}{n}(S_n - S) \\
&\quad + \frac{1}{n+1}[(S_1 - S) + (S_2 - S) + \cdots + S_{n-1} - S)] \\
&\quad + \frac{S_n + S_{n+1} - 2S}{n+1}
\end{aligned} \tag{A11}$$

There are two cases.

(a) When n is even, $(S_1-S)+(S_2-S)+\cdots+(S_{n-1}-S)<0$, we have

$$F(\bar{S}_n,\bar{S}_{n+1},S) < \frac{S_n-S}{n}+\frac{S_n+S_{n+1}-2S}{n+1} < S_n+S_{n+1}-2S \quad \text{for } n>\bar{N} = |S_n-S|-|S_{n+1}-S| = F(S_n,S_{n+1},S) \tag{A12}$$

where $\bar{N}$ is an integer, satisfying

$$(S_{\bar{N}}-S)+(S_{\bar{N}+1}-S)+\frac{S_{\bar{N}+1}-S}{\bar{N}-2}>0 \tag{A13}$$

which can be reached since S_n, S are bounded, and $(S_{\bar{N}}-S)+(S_{\bar{N}+1}-S)>0$ for all n.

(b) When n is odd, $(S_2-S)+\cdots+(S_{n-1}-S)<0$, we have

$$\begin{aligned} F(\bar{S}_n,\bar{S}_{n+1},S) &< \frac{2n+1}{n(n+1)}(S_1-S)+\frac{S_n-S}{n}+\frac{S_n+S_{n+1}-2S}{n+1} \\ &< \frac{2n+2}{n(n+1)}(S_1-S)+\frac{S_n-S}{n}+\frac{S_n+S_{n+1}-2S}{n+1} \\ &= \frac{2}{n}(S_1-S)+\frac{S_n-S}{n}+\frac{S_n+S_{n+1}-2S}{n+1} \\ &< S_n+S_{n+1}-2S \quad \text{for } n>\bar{N} \\ &= |S_n-S|-|S_{n+1}-S| \\ &= F(S_n,S_{n+1},S) \end{aligned} \tag{A14}$$

where $\bar{N}$ is an integer, satisfying

$$(S_{\bar{N}}-S)+(S_{\bar{N}+1}-S)+\frac{S_{\bar{N}+1}-2S_1+S}{\bar{N}-2}>0 \tag{A15}$$

which is possible since S_n, S are bounded, and $(S_{\bar{N}}-S)+(S_{\bar{N}+1}-S)>0$ for all n. This finishes the proof for Part (ii).

References

[1] Glauert, M. B., 1956, "The Wall Jet," J. Fluid Mech., **1**, pp. 625–643.
[2] Bakke, P., 1957, "An Experimental Investigation of a Wall Jet," J. Fluid Mech., **2**, pp. 467–472.
[3] Poreh, M., Tsuel, Y. G., and Cermak, J. E., 1967, "Investigation of a Turbulent Radial Wall Jet," ASME Trans. J. Appl. Mech., **6**, pp. 457–463.
[4] Yih, C. S., 1959, "Two Solutions for Inviscid Rotational Flow With Corner Eddies," J. Fluid Mech., **5**, pp. 36–40.
[5] Phares, D. J., Smedley, G. T., and Flagan, R. C., 2000, "The Inviscid Impingement of a Jet With Arbitrary Velocity Profile," Phys. Fluids, **12**, pp. 2046–2055.
[6] Lee, J. A., Burggraf, O. R., and Conlisk, A. T., 1998, "On the Impulsive Blocking of a Vortex Jet," J. Fluid Mech., **369**, pp. 301–331.
[7] Xu, Z., 2004, "Experimental and Analytical Modeling of High Intensity Winds," Ph.D. thesis, University of Western Ontario, Ontario.
[8] Wang, Y. M., 1994, *Mine Aerodynamics and Ventilation Systems*, Metallurgical Industry, Beijing, in Chinese.
[9] Spiegel, M., and Liu, R. J., 1968, *Mathematical Handbook of Formulas and Tables*, McGraw-Hill, New York.
[10] White, F. M., 1991, *Viscous Fluid Flow*, 2nd ed., McGraw-Hill, New York.
[11] Schlichting, H., 1979, *Boundary-Layer Theory*, 7th ed., McGraw-Hill, New York.
[12] Kumada, M., and Mabuchi, I., 1970, "Studies on the Heat Transfer of Impinging Jet," Bull. JSME, **13**, pp. 77–85.
[13] Beltaos, S., and Rajaratnam, N., 1973, "Plane Turbulent Impinging Jets," J. Hydraul. Res., **11**, pp. 29–59.
[14] Landreth, C. C., and Adrian, R. J., 1990, "Impingement of a Low Reynolds Number Turbulent Circular Jet," Exp. Fluids, **9**, pp. 74–84.
[15] Sheen, H. J., Chen, W. J., and Jeng, S. Y., 1996, "Recirculation Zones of Unconfined and Confined Annular Swirling Jets," AIAA J., **34**, pp. 572–579.
[16] Rubel, A., 1983, "Inviscid Axisymmatric Jet Impingement With Recirculating Stagnation Regions," AIAA J., **21**, pp. 351–357.
[17] Donaldson, C. D., and Snedeker, R. S., 1971, "A Study of Free Jet Impingement. Part 1. Mean Properties of Free and Impinging Jets," J. Fluid Mech., **45**, pp. 281–319.